 doi:10.20944/preprints201712.0106.v1

Article

Chemical Vapour Deposition Graphene Field-Effect Transistors for Detection of Human Chorionic Gonadotropin Cancer Risk Biomarker

Carrie Haslam[1], Samar Damiati[2], Toby Whitley[1], Paul Davey[1], Emmanuel Ifeachor[1] and Shakil A. Awan[1,*]

[1] School of Computing, Electronics and Mathematics, Faculty of Science and Engineering, University of Plymouth, PL4 8AA, UK;
[2] Department of Biochemistry, Faculty of Science, King Abdulaziz University (KAU), Jeddah, Saudi Arabia;
* Correspondence: shakil.awan@plymouth.ac.uk; Tel.: +44(0)1752 586 325

Abstract: We report on the development of chemical vapour deposition (CVD) based graphene field effect transistor (GFET) immunosensors for the sensitive detection of Human Chorionic Gonadotropin (hCG), a glycoprotein risk biomarker of certain cancers. The GFET sensors were fabricated on Si/SiO_2 substrate using photolithography with evaporated chromium and sputtered gold contacts. GFET channels were functionalized with a linker molecule to immobile anti-hCG antibody on the surface of graphene. Binding reaction of the antibody with varying concentration levels of hCG antigen demonstrated the limit of detection of the GFET sensors was ~0.1 pg/mL using four-probe electrical measurements. We also show annealing can significantly improve the carrier transport properties of GFETs and shift the Dirac point (Fermi level) with reduced p-doping in back-gated measurements. The developed GFET biosensors are generic and could find applications in a broad range of medical diagnostics in addition to cancer, such as neurodegenerative (Alzheimer's, Parkinson's and Lewy body) and cardiovascular disorders.

Keywords: graphene; electrochemical biosensors; cancer; diagnosis; electrical detection; alzheimer's disease; dementia; neurodegenerative disorders; cardiovascular; blood biomarkers; antibodies; proteins

1. Introduction

Since the discovery and isolation of graphene from graphite in 2004, the two-dimensional material has shown potential to revolutionise many technological areas owing to its remarkable electrical, optical, mechanical and thermal properties [1-3]. Graphene is a mono-atomic, planar network of sp^2-bonded carbon atoms arranged in a honeycomb lattice. In particular, its chemical stability, low electrical noise, significant surface-to-volume ratio, biocompatibility and field-effect make graphene potentially an ideal platform for a variety of biosensing applications [4]. The extraordinary surface-to-volume ratio of graphene facilitates a high density of disease specific biomarkers to be chemically functionalised onto its surface via covalent or non-covalent immobilisation techniques. A key benefit of the latter is that the electrical transport properties of graphene are not degraded as the mobility and carrier properties are maintained. This can enhance the sensitivity of the biosensor and thereby improve its limit of detection (LoD). Currently, a number of biosensor techniques are being explored to detect the presence of a given biomarker, such as electrical, optical, resonant, acoustical, quartz crystal microbalance and surface plasmon resonance

 doi:10.20944/preprints201712.0106.v1

(SPR) [5]. Whilst each technique has its advantages and disadvantages, the electrical technique we are exploring offers some key benefits that make it a prime candidate for eventual point-of-care (PoC) applications in the detection of specific cancer biomarkers and early diagnosis. These include, label-free detection, high sensitivity, multiplexing, low-cost and integration with a range of existing electronic systems. In contrast with our field-effect transistor (FET) biosensors, there are also other electrical techniques, such as cyclic voltammetry (CV), impedimetry and ampreometry functioning to detect a variation in resistance and/or capacitance, that may be comparable to the FET approach in terms of sensitivity. The developed FETs will be generic sensors and are therefore expected to have numerous other applications ranging from neurodegenerative disorders (ND), such as Alzheimer's [6] and other dementias, and cardiovascular to infectious diseases and environmental monitoring.

Here we report on the chemical vapour deposition (CVD) graphene field-effect transistor (GFET) biosensors aimed at detecting the presence of Human Chorionic Gonadotropin (hCG) protein biomarkers in samples from patients at different stages of disease progression. The proof-of-concept GFETs were functionalized with monoclonal anti-hCG antibodies for the detection of hCG protein biomarkers, label-free. hCG is a glycoprotein hormone (*37*-kDa) and its concentration level serves as a clinical marker associated with testicular, pancreatic and prostate cancer [7-9], as well as pregnancy. As with many diseases, early cancer recognition and diagnosis can be critical for treatment and management to be effective, as well as enabling optimum health care provision and potentially opening novel routes to be investigated to prevent the development of the disease [10-12]. There is therefore an urgent need to develop diagnostic sensors and analytical tools for the accurate identification and early diagnosis of cancer. hCG is composed of two subunits α and β, which are non-covalently linked by hydrophobic and ionic interactions. The α subunit is known to be common and the β subunit is unique to hCG, conferring biological activity to the hormone. The length of the β subunit is composed of 145 amino acids [13-17]. As a pregnancy biomarker hCG is usually secreted by the trophoblast cells of the placenta peaks at ~ 10 weeks into the human gestation period. The chief function of hCG is considered to maintain the corpus luteum and promote the production of progesterone during pregnancy by the ovarian granulosa cells, whilst endorsing foetal growth [18-22]. A typical, commercial biosensor that is designed to detect hCG and establish pregnancy exhibits sensitively down to a nano-molar range [23]. It has been previously estimated that 95% of pregnancies can be detected at a sensitivity of 12.4 mIU/mL at the time of an expected menstrual period [24-25]. Our GFET biosensors detailed here exhibit a significantly lower limit of detection of 0.1 pg/mL (determined using a 4-probe electrical technique) compared to a commercial biosensor designed specifically for hCG detection. There are number of other studies that have investigated hCG biomarker to analyse the necessary LoD of their sensors, e.g. Heideman *et al.* [26], where they developed a Mach-Zehnder interferometer (MZI) immunosensor, based on a silicon substrate with a detection limit of 50pM [[26,27]. In respect to hCG detection via graphene, Teixeira *et al.* [15] applied chemically-modified multi-layer epitaxial graphene to serve as the sense electrode (functionalized with APTES). The device displayed a LoD of 0.62 ng/mL [15]. In addition, Teixeira *et al* produced an immunosensor based on screen-printed electrodes (SPEs), with graphene functioning as the working electrode to detect hCG. The LoD was determined to be 0.286 pg/mL [28]. To the best of our knowledge, there has not yet been a CVD graphene biosensor reported that has been able to detect hCG concentration at the ~0.1 pg/mL level. The developed GFET biosensors will also need to be validated against the gold standard in the field, that of immunoassay enzyme-linked

 doi:10.20944/preprints201712.0106.v1

immunosorbent assay (ELISA). In addition, since performing ELISA tests can be time consuming, requires high level of operator expertise and complex equipment, making it expensive, we envisage that GFET biosensors could present a potential low-cost, fast, accurate and reliable alternative technology platform.

2. Materials and Methods

Monolayer Graphene on a SiO_2/Si wafer was purchased from Graphenea (Spain). The required chemicals applied for GFET fabrication were photoresist (PR), lift-off resist (LoR), Microposit developer and Microposit remover, all purchased from A-Gas Electronic Materials (Warwickshire, UK).

The hCG antigen and complementary anti-hCG monoclonal antibody were purchased from Abcam *(UK).* The stock were stored at −20 °C. Linker molecule 1-pyrenebutanoic acid succinimidyl ester (Pyr-NHS) and bovine serum albumin (BSA) blocking solution were purchased from Sigma Aldrich *(Dorset, UK).* Phosphate-Buffered Saline (PBS) tablets were purchased from Sigma Aldrich *(Germany).*

Electrical characterisation and analysis were implemented under ambient conditions via a Keysight B1500A semiconductor device parameter analyser, in conjunction with a Cascade Microtech MPS150 probe station *(Thiendrof, Germany).* Current-voltage measurements (I_D-V_D and I_D-V_G) were executed as a function of gate voltage (V_G) from - 100 V to + 100 V. The I_D-V_D curves were acquired from - 100 mV to + 100 mV. The I_D-V_D and I_D-V_G curves were measured for each separate functionalisation stage.

Graphene characterisation was performed using an XPLORA Raman spectroscopy system *(HORIBA, UK).* The XPLORA system operated at a wavelength of 532 nm, with ~ 4 mW of incident power. The XPLORA Raman system was combined with an OLYMPUS BX41 microscope *(Olympas, Japan).*

To define and develop the necessary graphene channels and metallic contacts of Chromium (Cr) and Gold (Au), the Mask aligner J500/VIS *(OAI optical associates Inc)* was deployed. A conventional fan oven *(WTB binder, Germany)* was employed to perform necessary annealing processes, as well as for pre- and post-baking stages during the photolithography processes. The Hotplate SH8 *(STUART SCIENTIFIC)* and Ultrasonic Cleaner (*CBEST, US*) were used for pre- and post-baking procedures and PR removal, respectively. An Argon (Ar) plasma etching technique was used for graphene channel formation by means of a three target, 6-inch sputtering machine (*Nordiko Limited, UK).* To aid in the formation of robust, metallic electrodes, an Edwards Thermal Evaporator was deployed for the evaporation of Cr.

2.1. Fabrication of CVD Graphene FETs

The GFETs were fabricated using high quality CVD graphene to form transducer channels on Si/SiO_2 substrate. A conventional photolithographic patterning and metal lift-off technique was used to form the necessary graphene channels, as well as the source, drain and voltage sense electrodes. The fabrication process involved spin-coating the CVD graphene samples with Lift-off Resist (LOR) at 3000 rmp for a few seconds. The samples were then placed in a fan oven for pre-baking. The purpose of the pre-bake was to densify the LOR to assist with the formation of clear, graphene channels. Subsequently, the samples were dried at an ambient temperature. Next, the samples were

 doi:10.20944/preprints201712.0106.v1

spin-coated with a layer of positive Photoresist (PR). Immediately after PR deposition, the samples were post-baked on a hotplate. The hotplate solidifies the PR and removes any solvents remaining on the samples. This process generated ~ 500 nm of PR film on the surface of graphene. Successively, the coated samples were then positioned in a mask aligner and exposed to ultra-violet (UV) radiation for lithographic patterning of graphene channels. The UV exposed samples were also submerged in a chemical developer before being placed in a vacuum chamber to dry. Alternatively, the samples can be left to dry at ambient temperature, outside of the vacuum chamber. An additional post-baking stage was applied to the samples following the drying and placed on a hotplate under an intermittent deep ultraviolet source (DUV). This exposure to DUV can reduce the quantity of PR/PMMA residue on the substrate surface prior to plasma etching, whilst reducing contact resistance.

The chemically developed and dried samples were transferred into a sputtering machine and exposed to Ar plasma etching for few minutes. Throughout the process, the inert Ar gas functions as the gaseous etchant and removes the exposed regions of graphene, whilst leaving behind the shaped graphene channels (previously coated and protected with PR). Graphene shaping is effectively complete after an etching time of a few minutes at high power. The sputtering machine was also used to sputter and form the associated metallic electrodes, 30 nm of Au. Following successful shaping, the samples were transferred to a chemical remover to dissolve the LoR and PR remaining on the substrate to expose the graphene channels. The samples were immersed in the chemical remover, whilst located in an ultrasonic bath for ~2 hour at ~60°C. The samples were subsequently rinsed and bathed in de-ionised water and transferred into a vacuum chamber to dry for few hours.

For the final stage of GFET fabrication, metallic Cr and Au electrodes were formed on the graphene channels. The samples were post-baked in a fan oven, instead of being irradiated with DUV. This post-baking stage is necessary to remove the solvents located within the PR and eliminate any additional water. Following photolithography, thermal evaporation of Cr was performed using an Edwards Thermal Evaporator for a few seconds. The Cr functions as an adhesive layer between graphene and the Au metallic contacts. The Cr target material was heated to ~2000°C and evaporated within a high vacuum. The heated coil of Cr is applied to form a thin film of ~5 nm on the surface of the graphene samples. The metallic contacts are fully formed after sputtering 30 nm of Au on the Cr film. After the Au sputtering process, the initial chemical remover step is repeated and the final samples are dried in a vacuum chamber for a few hours, prior to electrical characterisation.

For this study a number of CVD graphene samples were fabricated. Each sample consisted of fifteen GFET devices (with an area of ~1 cm^2) in total, i.e. five GFET devices consisted of five asymmetric Cr/Au voltage sense electrodes with an associated graphene channel length of 720 μm, whereas the remaining ten GFET devices consisted of six symmetric voltage sense electrodes with a channel length of 300 μm, as shown in Fig. 1. The width of all GFET channels was fixed at 80 μm.

Preprints (www.preprints.org) | NOT PEER-REVIEWED | Posted: 15 December 2017 doi:10.20944/preprints201712.0106.v1

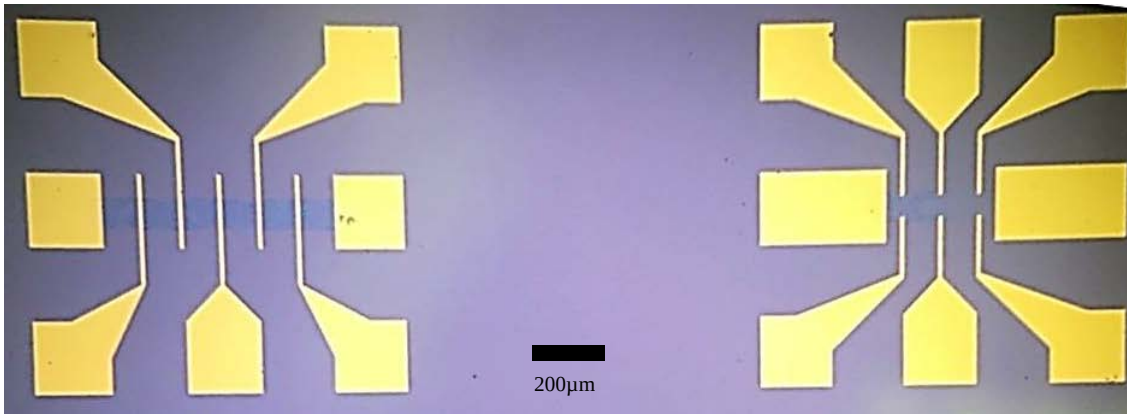

Figure 1: Graphene FET devices with asymmetric (left) and symmetric (right) voltage sense electrodes. Graphene channels, in the central regions of the FET devices, have a dark blue contrast compared to the Si/SiO_2 substrate.

3. Results

3.1. Characterisation of CVD Graphene using Raman Spectroscopy

Raman spectroscopy was performed on two representative CVD samples to analyse the quality of graphene and to estimate various properties, such as number of layers [29], doping and residues from the fabrication process. Random spot Raman measurements were carried out at the central region of bare samples. The Raman spectra were measured with a 10X objective, under ambient conditions with an incident power of ~ 4 mW and a wavelength of 532 nm. Figure 2 shows Raman spectra from the two samples with an intensity ratio of the 2D peak to G peak of I(2D)/I(G) ~ 2 and one sample shows a significant D peak, whereas it is absent in the other. The intensity ratio I(2D)/I(G), position and full width half maximum (FWHM) of the G and 2D peaks confirm presence of monolayer graphene. The presence and intensity of the D peak in one of the samples also indicates that the graphene in that sample contains defects. Raman mapping of a few regions of the graphene wafer (before it was diced into 1cm^2 samples) confirmed majority of the regions consisted of mono-layer graphene.

3.2. Electrical Characterisation of GFETs

The GFETs were characterized using 2-probe, 4-probe and back-gated measurements under ambient conditions. The bare GFETs (i.e. without any biomolecule functionalization) were first measured to extract the I_D-V_D characteristics of the fifteen devices on each 1 cm^2 sample. A comparison between 2-probe, 4-probe and back-gated data enabled us to extract the contact resistance, mobility and sheet resistance of the graphene channels within the GFET devices. A typical 4-probe I_D-V_D and I_D-V_G measurements from a GFET sensor using a Keysight parameter analyser interfaced to a Cascade probe station is shown in Fig. 3. The I_D-V_D data shows approximate linear response over the ± 60 mV range and a slight non-linearity beyond this range probably due to adsorbed water molecules on the surface of the graphene channel and charge traps in the Si/SiO_2 substrate. This is further confirmed from the I_D-V_G data which shows a characteristic hysteretic behavior due to the presence of polar molecules on the surface of graphene and charge traps. The Dirac point is found to vary from 50 V to 80 V depending on the voltage sweep and its positive magnitude indicates the graphene channel is p-doped. The 4-probe resistance of the graphene channel is found to be ~700 Ω, whereas the mobility is approximately 1200 cm^2/Vs.

Preprints (www.preprints.org) | NOT PEER-REVIEWED | Posted: 15 December 2017 doi:10.20944/preprints201712.0106.v1

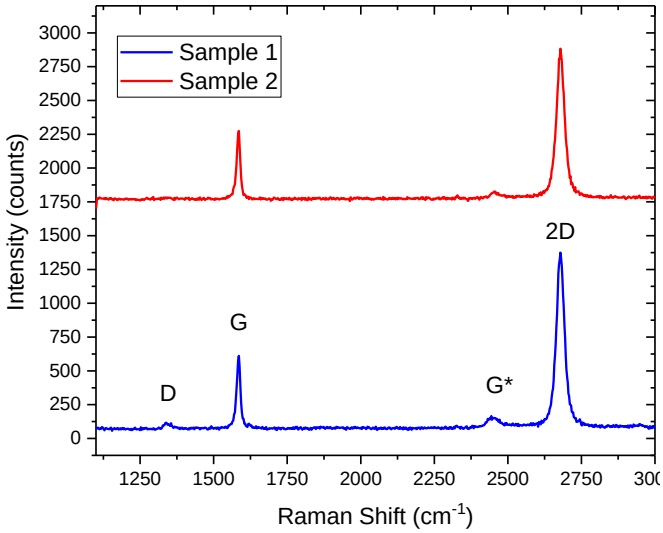

Figure 2: Raman Spectra of quality and defected CVD graphene before being deployed as the transducer element in a GFET biosensor. The defected sample (blue) shows a prominent D-band.

We have also explored the effect of annealing on our devices in order to improve the overall performance of the bare GFET sensors. Figure 4 displays the results from one device before and after annealing. Before annealing the device showed relatively low conduction level and its Dirac point was in excess of 40 V. However, after annealing the sample, the Dirac point could now be discerned and shifted to approximately 23 V (with p-type doping). This is likely due to desorption of oxygen and water molecules from the surface of graphene [30-32]. In pristine graphene, the Dirac point would ideally be located at zero gate voltage. A Dirac point situated relatively far from the zero point indicates unintentional doping, which could be due to the fabrication process. The location of the Dirac point is dependent on the difference between the work function of the gate, metallic contacts, and the graphene channel, as well as doping and the presence of biomolecules adsorbed on the surface [33]. From a knowledge of the Dirac point and shape of the I_D-V_G curve near its vicinity, a number of properties of the channel can be estimated, such as mobility, doping, defects etc.

Preprints (www.preprints.org) | NOT PEER-REVIEWED | Posted: 15 December 2017 doi:10.20944/preprints201712.0106.v1

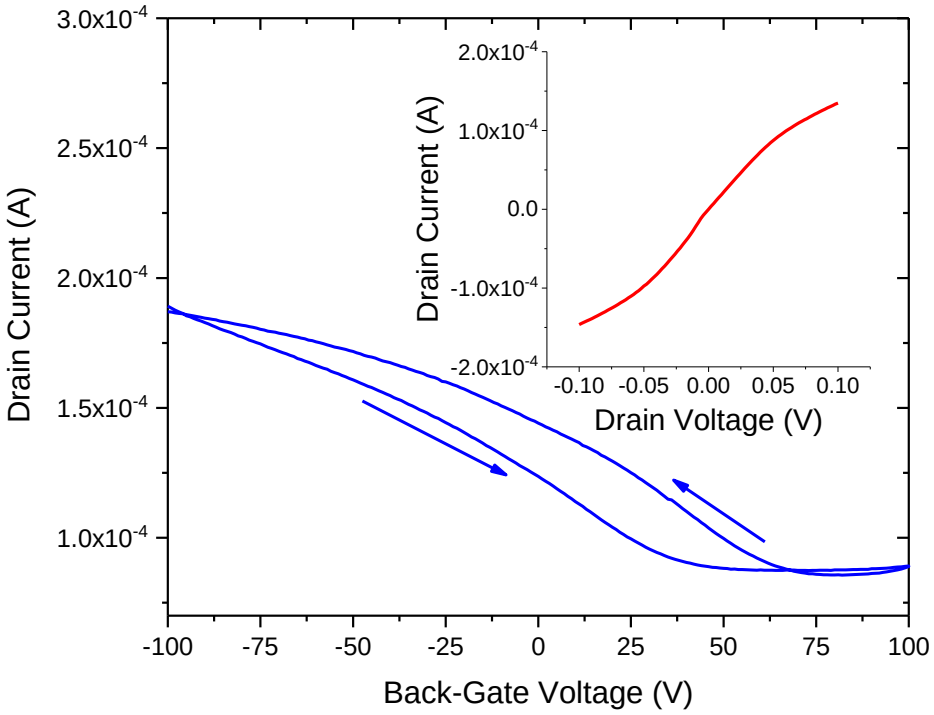

Figure 3: I_D-V_G and the corresponding I_D-V_D (inset) of a CVD graphene FET sensor. The arrows indicate forward and reverse sweep of the back-gate voltage showing hysteretic behavior.

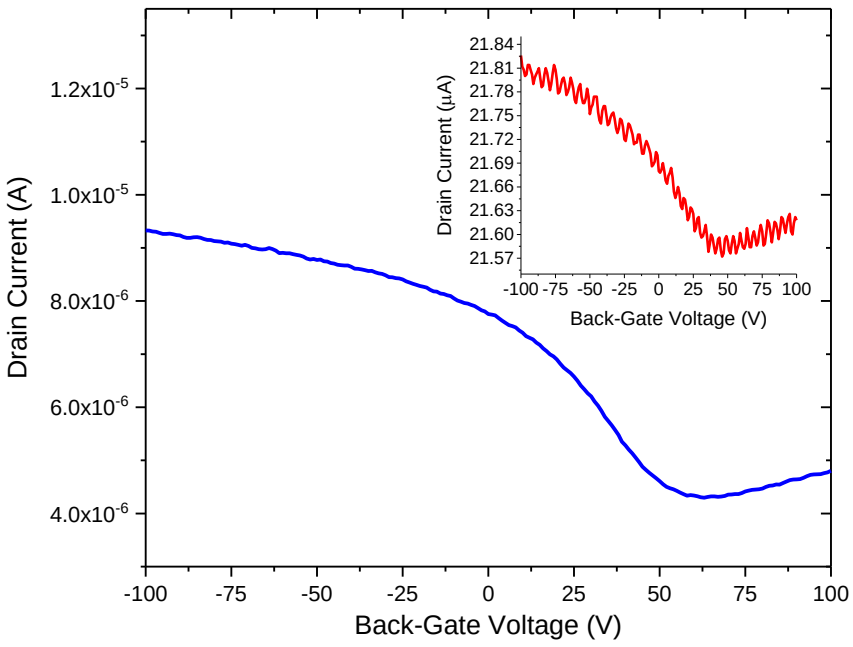

Figure 4: Annealed I_D-V_G curve of a CVD graphene FET and its corresponding I_D-V_G (inset) before annealing.

 doi:10.20944/preprints201712.0106.v1

3.3. Functionalisation of GFETs

To facilitate antibody (Ab) immobilization, we used a linker molecule Pyr-NHS ester. The linker retains a succinimidyl ester group, which interacts with the amino groups on the anti-hCG Ab surface to generate a stable, amide bond. In addition, the Pyr-NHS has an aromatic pyrenyl group, which can strongly interact with the graphene surface, via a non-covalent π-π stacking. Non-covalent binding is dependent on physical adsorption of the biomolecule, using hydrophobic, hydrophilic, electrostatic and van der Waals interactions. Thus, Pyr-NHS ester causes the pyrene group at one end of the linker to strongly bind to the graphene surface via π-π interactions and the succinimidyl ester group will covalently react with the amino group (NH_2) of the Ab without requiring a high pH [34]. The non-covalent attachment of Pyr-NHS ester with graphene does not disrupt the electrical properties of graphene, whereas covalent bonding can lead to scattering and the introduction of impurities in the graphene sp^2 lattice. This type of immobilisation typically leads to a self-assembled monolayer (SAM) of molecules on the surface of graphene, although the Abs may remain randomly orientated.

The GFET devices were biologically modified and converted into biosensors via the drop casting of biomolecules. Initially, Pyr-NHS ester linker molecules were applied to cover the surface of the graphene channels at a concentration of 2 mM. The samples were incubated at low temperature for a few hours before rinsing with PBS and drying at ambient temperature. Once the samples were dry, electrical characterisation was performed. Following attachment of Pyr-NHS ester and electrical characterisation, anti-hCG Ab was applied to the samples and again incubated before rinsing with PBS and drying at ambient temperature. The same process was repeated for BSA deposition. Finally, hCG antigen was applied to the samples at a concentration ranging from 0.1 pg/mL to 1 ng/mL and characterised using 4-probe electrical measurements. Samples were then incubated at ambient conditions for 1 hour, prior to a PBS rinse. Figure 5 illustrates the steps involved within the functionalisation process.

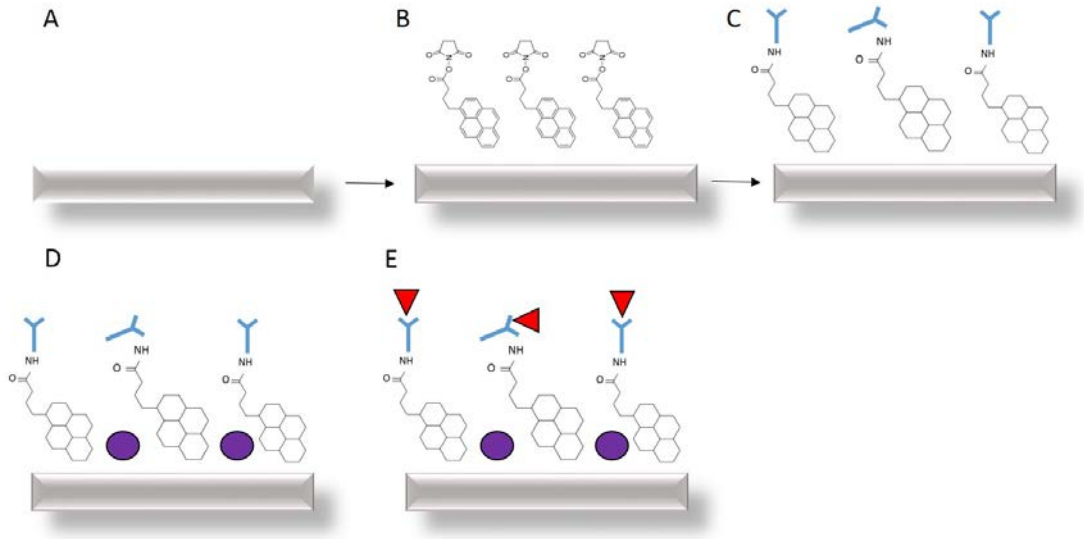

Figure 5: GFET functionalisation and antigen detection stages for (A) bare graphene (B) non-covalent attachment of Pyr-NHS ester linkers with graphene (C) anti-hCG antibody (light blue) attachment to the linkers (D) BSA blocking (dark blue) and (E) hCG antigen (red) binding with the antibody. Each stage is characterised using 4-probe electrical measurements of I_D-V_D and I_D-V_G.

Preprints (www.preprints.org) | NOT PEER-REVIEWED | Posted: 15 December 2017 doi:10.20944/preprints201712.0106.v1

3.4. Atomic Force Microscopy of Functionalised GFETs

Further characterisation of the functionalised GFETs was performed using Atomic Force Microscopy (AFM, *Pacific Nanotechnology* and probe tips from *Nano World*). Multiple AFM images were generated in respect to the various necessary functionalisation steps. The difference in height and morphology at hCG functionalisation stage is displayed in Figure 6. The AFM image illustrates the successful immobilisation of Pyr-NHS linker, Ab, BSA and the corresponding hCG antigen molecules on the surface of the graphene FETs. The hCG antigen is measured to be ~7-10 nm in height.

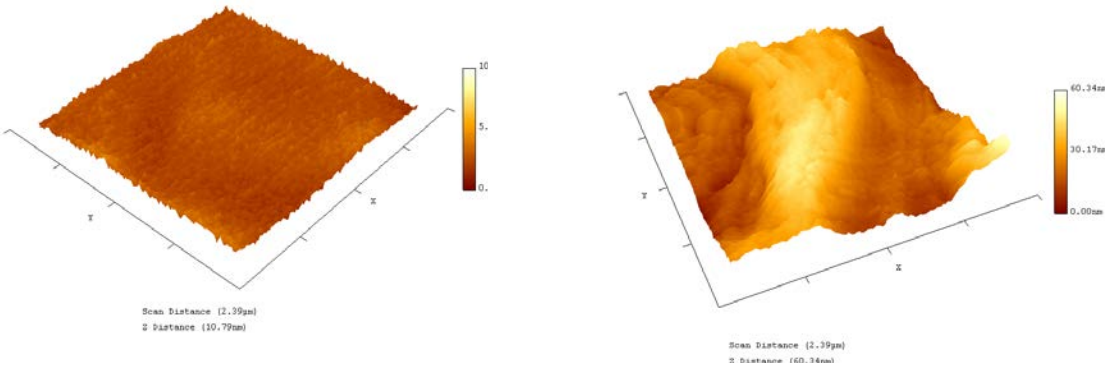

Figure 6: AFM image of bare graphene on Si/SiO2 (left) and immobilised with Pyr-NHS linker, Ab, BSA and the corresponding hCG antigen (right).

3.5. Scanning Electron Microscopy of Functionalised GFETs

SEM Image (using a JOEL JSM-7001F) shows a GFET device with 10 pg/mL of hCG antigen on the surface of graphene, including immobilisation of Pyr-NHS ester linker, Ab and BSA. The image

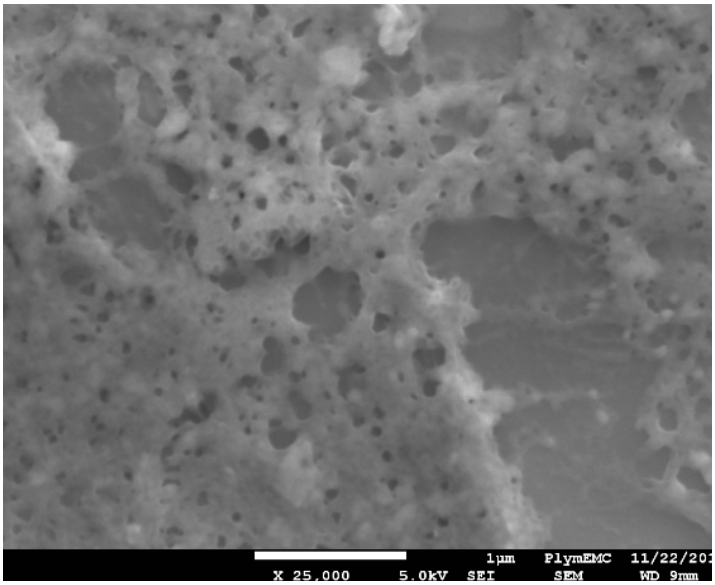

Figure 7: SEM image displaying bare graphene immobilised with Pyr-NHS linker, Ab, BSA and the corresponding hCG antigen. Scale bar is 1 µm.

Preprints (www.preprints.org) | NOT PEER-REVIEWED | Posted: 15 December 2017 doi:10.20944/preprints201712.0106.v1

(taken at 25,000 times magnification) shows hCG appearance to be foam like with relatively large voids over the 5μm × 5μm region. The hCG appears also not to be uniformly distributed, indicating further optimisation may be needed to achieve a uniform distribution of the antigen on the surface of graphene to enable consistent and repeatable response of the GFET biosensors.

3.6. Detection of hCG concentration

The fabricated GFET sensors were characterised using 4-probe electrical measurements at each stage of the functionalisation and binding interactions of the anti-hCG antibody with hCG antigen at varying concentration levels of the latter. All measurements were performed in ambient conditions. Figure 8 shows the response curves of two GFET biosensors when exposed to 1 pg/mL and 1 ng/mL hCG antigen. The corresponding changes in resistance at each stage and concentration levels are shown in Table 1. A striking feature of the results shown in Figure 8 and Table 1 is that whilst the change in resistance coefficient ΔR for 1 pg/mL is positive for all stages of the functionalisation, this is not the case for the 1 ng/mL concentration level. In this case, the coefficient is negative until antibody binding stage but then becomes positive. In addition, despite 3 orders-of-magnitude difference between the 1 pg/mL and 1 ng/mL concentration levels the change in resistance coefficient is ~114.1% and ~305%, respectively. In contrast, we measured ΔR~135.9% for 10 pg/mL and a LoD of the sensors to be ~0.1 pg/mL, as shown in Fig. 9. The response of the GFET sensors to hCG antigen concentration is found to be linear over the 1 pg/mL to 1 ng/mL range, as shown in Fig. 9. The least-square linear fit to the measured GFET 4-probe resistance change shows reasonably good fit with R^2 ~0.95. The corresponding sensitivity of the GFET biosensors is found to be ~(66.7±15)% / decade of hCG concentration over the 1 pg/mL to 1 ng/mL range. This represents a significant sensitivity level for hCG antigen detection. However, it is worth highlighting that our GFET biosensors have not yet been optimised for numerous parameters (mobility etc.) to achieve even higher sensitivity levels and lower detection limits. These aspects are currently being explored and will be reported on in subsequent future publications.

The data in Table 1 for the measured 4-probe resistance of the GFET sensors at 1 pg/mL and 1 ng/mL concentration levels also includes the change in resistance coefficient ΔR. This is calculated relative to the two nearest stages, i.e. bare graphene to linker, linker to Ab, etc. Thus, sensitivity of the sensors can be estimated from ΔR for hCG (or change in resistance from BSA to the hCG analyte).

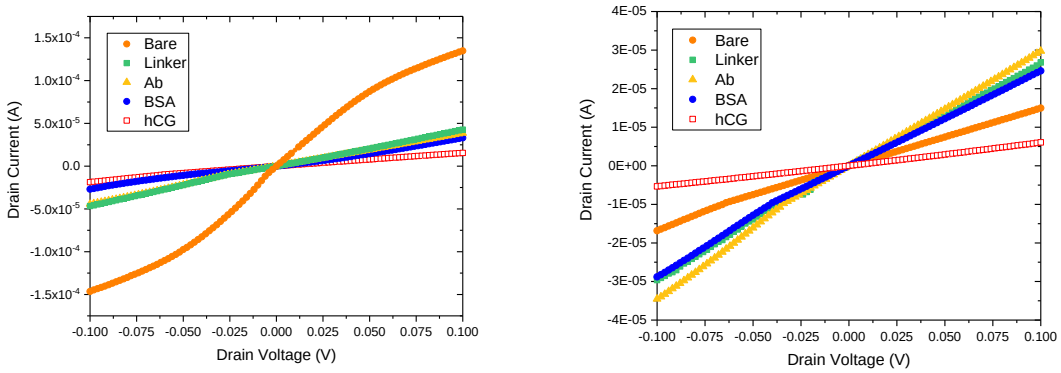

Figure 8: Characteristic I_D-V_D curves from the GFET sensors at different stages of biomolecule exposure for 1pg/mL (left) and 1ng/mL (right) hCG concentration levels.

Preprints (www.preprints.org) | NOT PEER-REVIEWED | Posted: 15 December 2017 doi:10.20944/preprints201712.0106.v1

Table 1. Summary of GFET resistance changes measured at different stages of the functionalisation process with 1pg/mL to 1ng/mL concentration of hCG antigen.

Stage	1pg/mL(Ω)	ΔR(%)	1ng/mL(Ω)	ΔR(%)
Bare	741.8	0	6686.3	0
Linker	2341.9	+215.7	3733.3	-44.2
Ab	2590.7	+10.6	3361.7	-11.1
BSA	3021.0	+16.6	4065.4	+20.9
hCG	6467.5	+114.1	16468.5	+305.1

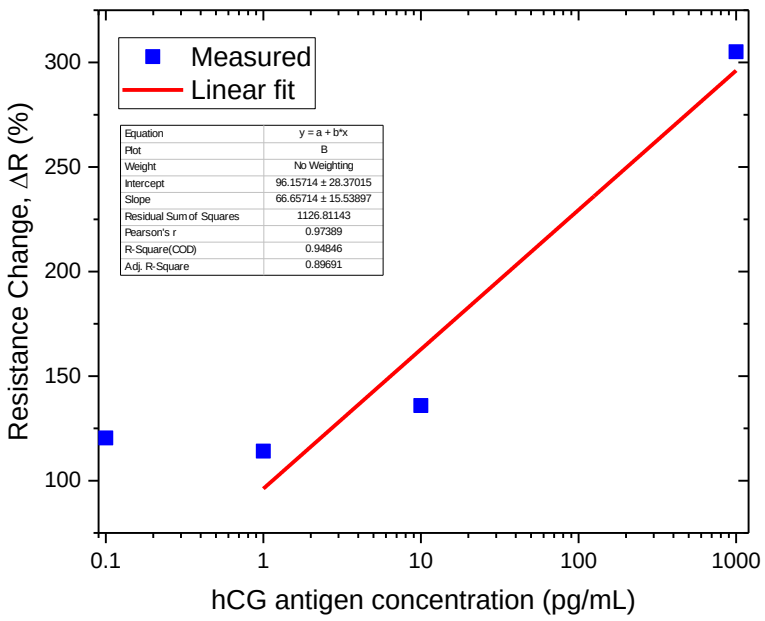

Figure 9: Measured resistance change coefficient with hCG concentration and a least-squares linear fit to the data from 1 pg/mL to 1 ng/mL range.

4. Discussion

The proof of concept CVD graphene FET biosensors have been characterised at all stages of the fabrication process (Raman, AFM, electrical) and functionalisation (Raman, AFM, SEM, electrical) to establish a robust and reproducible process for the development of the sensors. Our data presented in this study has demonstrated that proof-of-concept CVD graphene FETs can sensitively detect hCG antigen with approximately two orders of magnitude lower concentration level compared to commercial sensors. In addition, the GFET sensors can be operated in a resistive or back-gated mode

 doi:10.20944/preprints201712.0106.v1

and in the future we aim to compare the sensitivity of these two approaches. However, the data in Figure 8 shows clear characteristic curves for a resistive GFET sensor which we also observed for the 10 pg/mL concentration level of the hCG antigen. As shown in Figure 3, back-gated GFET sensor properties can be influenced due to the presence of water molecules on the surface of graphene and charge traps in the supporting substrate (in our case Si/SiO_2) leading to hysteretic effects. Therefore, a robust comparison of the resistive with back-gated GFET sensors will require careful device design and optimisation.

Annealing of the GFET biosensors showed remarkable improvements in their electrical performance, in terms of enhanced carrier transport properties and Dirac point shift due to oxygen and water molecules being desorbed from the surface of graphene. Work is currently underway to compare annealed devices with those that have been fabricated in the same batch but not annealed. In addition, all the results reported in this study are based on direct current (DC) 4-probe resistance measurements. We therefore anticipate further improvements in S/N can also be achieved using alternating current (AC) or radio-frequency (RF) detection techniques [35,36].

5. Conclusions

We have demonstrated the use of CVD graphene FETs on Si/SiO_2 substrate as sensitive immunosensors for the proof-of-concept detection of hCG antigen, with a LoD ~0.1 pg/mL. Although characteristic current-voltage response curves of the GFETs have been established, the sign of the resistance change coefficient ΔR has a strong dependence on the concentration level of the antigen. In addition, we have also shown that annealing the GFET sensors can significantly improve their performance and potentially lead to even more sensitive devices. In the near future the GFET biosensors will be explored for the detection of hCG biomarkers in case vs control samples from patients. Furthermore, in the next stage of development of the GFETs we will also investigate optimisation of the quality of CVD graphene, contact resistance and novel AC and RF detection techniques to enhance the sensitivity of the biosensors.

Acknowledgements

We acknowledge funding from the UK's Engineering and Physical Sciences Research Council (EPSRC) under contract number EP/M006301/1 and the University of Plymouth, GD105227. SD would like to thank University of Plymouth, UK, for a guest-researcher position in summer 2017.

References

1. Novoselov, K.S., et al., *Electric field effect in atomically thin carbon films.* Science, 2004. **306**(5696): p. 666-9.
2. Geim, A.K., *Graphene: status and prospects.* Science, 2009. **324**(5934): p. 1530-4.
3. Geim, A.K. and P. Kim, *Carbon wonderland.* Sci Am, 2008. **298**(4): p. 90-7.
4. Forsyth, R., A. Devadoss, and O.J. Guy, *Graphene Field Effect Transistors for Biomedical Applications: Current Status and Future Prospects.* Diagnostics (Basel), 2017. **7**(3).

5. Allsop, T., et al., *Real-time kinetic binding studies at attomolar concentrations in solution phase using a single-stage opto-biosensing platform based upon infrared surface plasmons.* Opt Express, 2017. **25**(1): p. 39-58.
6. World Alzheimer's Report 2016. Publisher, *Alzheimer's Disease International*, September 2016.
7. Sánchez, S., et al., *Toward a fast, easy, and versatile immobilization of biomolecules into carbon nanotube/polysulfone-based biosensors for the detection of hCG hormone.* Analytical chemistry, 2008. **80**(17): p. 6508-6514.
8. Sinosich, M.J., H. Torode, and D. Saunders, *Diagnosis and management of extrauterine pregnancies.* Australian and New Zealand journal of obstetrics and gynaecology, 1993. **33**(3): p. 307-311.
9. Santandreu, M., S. Alegret, and E. Fabregas, *Determination of β-HCG using amperometric immunosensors based on a conducting immunocomposite.* Analytica Chimica Acta, 1999. **396**(2): p. 181-188.
10. Yang, W., et al., *Carbon nanomaterials in biosensors: should you use nanotubes or graphene?* Angewandte Chemie International Edition, 2010. **49**(12): p. 2114-2138.
11. Chen, A. and S. Chatterjee, *Nanomaterials based electrochemical sensors for biomedical applications.* Chemical Society Reviews, 2013. **42**(12): p. 5425-5438.
12. Pumera, M., *Graphene in biosensing.* Materials today, 2011. **14**(7): p. 308-315.
13. Pierce, J.G. and T.F. Parsons, *Glycoprotein hormones: structure and function.* Annual review of biochemistry, 1981. **50**(1): p. 465-495.
14. Stenman, U.-H., et al., *The classification, functions and clinical use of different isoforms of HCG.* Human reproduction update, 2006. **12**(6): p. 769-784.
15. Teixeira, S., et al., *Epitaxial graphene immunosensor for human chorionic gonadotropin.* Sensors and Actuators B: Chemical, 2014. **190**: p. 723-729.
16. Netto, G.J. and J.I. Epstein, *Chapter 16 - Immunohistology of the Prostate, Bladder, Kidney, and Testis A2 - Dabbs, David J*, in *Diagnostic Immunohistochemistry (THIRD EDITION)*. 2011, W.B. Saunders: Philadelphia. p. 593-661.
17. Cole, L.A., *Biological functions of hCG and hCG-related molecules.* Reproductive Biology and Endocrinology : RB&E, 2010. **8**: p. 102-102.
18. Bahadır, E.B. and M.K. Sezgintürk, *Applications of electrochemical immunosensors for early clinical diagnostics.* Talanta, 2015. **132**: p. 162-174.
19. Tsampalas, M., et al., *Human chorionic gonadotropin: A hormone with immunological and angiogenic properties.* Journal of Reproductive Immunology, 2010. **85**(1): p. 93-98.
20. Cole, L.A., *hCG, five independent molecules.* Clinica chimica acta, 2012. **413**(1): p. 48-65.
21. Korevaar, T.I.M., et al., *Reference ranges and determinants of total hCG levels during pregnancy: the Generation R Study.* European Journal of Epidemiology, 2015. **30**(9): p. 1057-1066.
22. Larsen, J., et al., *Human chorionic gonadotropin as a measure of pregnancy duration.* International Journal of Gynecology & Obstetrics, 2013. **123**(3): p. 189-195.
23. Bahadır, E.B. and M.K. Sezgintürk, *Applications of commercial biosensors in clinical, food, environmental, and biothreat/biowarfare analyses.* Analytical Biochemistry, 2015. **478**(Supplement C): p. 107-120.
24. Cole, L.A., et al., *Accuracy of home pregnancy tests at the time of missed menses.* American journal of obstetrics and gynecology, 2004. **190**(1): p. 100-105.

25. Gnoth, C. and S. Johnson, *Strips of Hope: Accuracy of Home Pregnancy Tests and New Developments.* Geburtshilfe und Frauenheilkunde, 2014. **74**(7): p. 661-669.
26. Heideman, R., R. Kooyman, and J. Greve, *Performance of a highly sensitive optical waveguide Mach-Zehnder interferometer immunosensor.* Sensors and Actuators B: Chemical, 1993. **10**(3): p. 209-217.
27. Fan, X., et al., *Sensitive optical biosensors for unlabeled targets: A review.* Analytica Chimica Acta, 2008. **620**(1): p. 8-26.
28. Teixeira, S., et al., *Label-free human chorionic gonadotropin detection at picogram levels using oriented antibodies bound to graphene screen-printed electrodes.* Journal of Materials Chemistry B, 2014. **2**(13): p. 1852-1865.
29. Ferrari, A.C., et al., *Raman spectrum of graphene and graphene layers.* Physical review letters, 2006. **97**(18): p. 187401.
30. Tien, D.H., et al., *Characterization of Graphene-based FET Fabricated using a Shadow Mask.* Scientific reports, 2016. **6**: p. 25050.
31. Chen, S., et al., *Adsorption/desorption and electrically controlled flipping of ammonia molecules on graphene.* New Journal of Physics, 2010. **12**(12): p. 125011.
32. Joshi, P., et al., *Intrinsic doping and gate hysteresis in graphene field effect devices fabricated on SiO2 substrates.* Journal of Physics: Condensed Matter, 2010. **22**(33): p. 334214.
33. Chen, F., J. Xia, and N. Tao, *Ionic screening of charged-impurity scattering in graphene.* Nano Letters, 2009. **9**(4): p. 1621-1625.
34. Huang, Y., et al., *Graphene-based biosensors for detection of bacteria and their metabolic activities.* Journal of Materials Chemistry, 2011. **21**(33): p. 12358-12362.
35. Awan, S., et al., *Transport conductivity of graphene at RF and microwave frequencies.* 2D Materials, 2016. **3**(1): p. 015010.
36. Awan, S., et al., *Coaxial electrical circuits for interference-free measurements*. 2011, IET.